



Thermal property prediction and measurement of organic phase change materials in the liquid phase near the melting point[☆]



William E. O'Connor, Ronald Warzoha, Rebecca Weigand, Amy S. Fleischer, Aaron P. Wemhoff*

Department of Mechanical Engineering, Villanova University, 800 Lancaster Ave., Villanova, PA 19085, USA

HIGHLIGHTS

- Liquid-phase thermal properties for five phase change materials were estimated.
- Various liquid phase and phase transition thermal properties were measured.
- The thermal diffusivity was found using a best path to prediction approach.
- The thermal diffusivity predictive method shows 15% agreement for organic PCMs.

ARTICLE INFO

Article history:

Received 20 February 2014
Received in revised form 18 June 2014
Accepted 11 July 2014

Keywords:

Phase change material
Statistical thermodynamics
Thermophysical properties
Differential scanning calorimetry
Transient plane source
Thermal diffusivity

ABSTRACT

Organic phase change materials (PCMs) are a popular choice for many thermal energy storage applications including solar energy, building envelope thermal barriers, and passive cooling of portable electronics. Since the extent of phase change during a heating or cooling process is dependent upon rapid thermal penetration into the PCM, accurate knowledge of the thermal diffusivity of the PCM in both solid and liquid phases is crucial. This study addresses the existing gaps in information for liquid-phase PCM properties by examining an approach that determines the best path to prediction (BPP) for the thermal diffusivity of both alkanes and unsaturated acids. Knowledge of the BPP will enable researchers to explore the influence of PCM molecular structure on bulk thermophysical properties, thereby allowing the fabrication of optimized PCMs.

The BPP method determines which of the tens of thousands of combinations of 22 different available theoretical techniques provides best agreement with thermal diffusivity values based on reported or measured density, heat capacity, and thermal conductivity for each of five PCMs (heneicosane, tricosane, tetracosane, oleic acid, and linoleic acid) in the liquid phase near the melting point. Separate BPPs were calibrated for alkanes based on heneicosane and tetracosane, and for the unsaturated acids. The alkane and unsaturated acid BPPs were then tested on a variety of similar materials, showing agreement with reported/measured thermal diffusivity within ~15% for all materials. The alkane BPP was then applied to find that increasing the length of alkane chains decreases the PCM thermal diffusivity, showing how the determination of the BPP can be used to aid in the prediction of how the molecular structure of organic PCMs influences PCM performance in energy storage applications.

© 2014 Elsevier Ltd. All rights reserved.

1. Introduction

Organic phase change materials (PCMs) have been proposed as a viable energy storage mechanism through solid–liquid phase change at the melting point temperature. This energy storage could have significant applications in solar energy [1–7], building envelope thermal barriers [8–16], and passive cooling of portable

electronics [17–19]. Since the extent of phase change during a heating or cooling process is dependent upon the amount of thermal penetration into the PCM, the thermal diffusivity of the PCM is an important thermophysical property for the viability of the material in an energy storage application.

The thermal diffusivity, α_{th} , is defined as

$$\alpha_{th} = \frac{\lambda}{\rho c_p} \quad (1)$$

where λ is thermal conductivity, ρ is mass density, and c_p is the mass-based heat capacity. Data regarding some of the solid and

[☆] Submitted for consideration for publication in *Applied Energy*.

* Corresponding author. Fax: +1 610 519 7312.

E-mail address: aaron.wemhoff@villanova.edu (A.P. Wemhoff).

Nomenclature

a_i, d_i	group contribution parameters, dimensionless	tck	critical temperature group contribution parameter, dimensionless
a_p	Peng–Robinson fluid model intermolecular potential parameter, J m^3	$tfp1k$	first-order melting temperature group contribution parameter, dimensionless
a_R	Redlich–Kwong fluid model intermolecular potential parameter, $\text{J m}^3 \text{K}^{0.5}$	$tfp2j$	second-order melting temperature group contribution parameter, dimensionless
a_S	Soave–Redlich–Kwong fluid model intermolecular potential parameter, J m^3	P	pressure, Pa
a_V	Van der Waals fluid model intermolecular potential parameter, J m^3	P_c	critical pressure, Pa
b_p	Peng–Robinson fluid model equivalent molecular volume, m^3	P_o	atmospheric pressure, Pa
b_R	Redlich–Kwong fluid model equivalent molecular volume, m^3	P_r	reduced pressure, dimensionless
b_S	Soave–Redlich–Kwong fluid model equivalent molecular volume, m^3	P_{rb}	reduced boiling point pressure, dimensionless
b_V	Van der Waals fluid model equivalent molecular volume, m^3	Q	canonical partition function, dimensionless
c_p	mass-based heat capacity, $\text{J}/(\text{kg K})$	R	ideal gas constant, $\text{J}/(\text{kmol K})$
C_{pl}	molar heat capacity, $\text{J}/(\text{mol K})$	T	temperature, K
$c_{p,st}$	mass-based heat capacity of sapphire sample, $\text{J}/(\text{kg K})$	T_b	boiling point temperature, K
D_s	difference in heat flow between empty reference pan and sample of interest, mW	T_c	critical temperature, K
D_{st}	difference in heat flow between empty reference pan and sapphire sample, mW	T_m	melting point temperature, K
E	reference calorimetric sensitivity, dimensionless	T_{rb}	reduced boiling point temperature, dimensionless
f, α	fluid model-dependent parameters, dimensionless	U	system internal energy, J
g	temperature ramp rate, $^{\circ}\text{C}/\text{min}$	V_s	saturated liquid molar volume, cm^3/mol
H	system enthalpy, J	W	weight for second-order groups (= 0 for 1st order, = 1 for 2nd order), dimensionless
h	Planck's constant, J s	W_s	weight of sample of interest, mg
k_B	Boltzmann's constant, J/K	W_{st}	weight of sapphire sample, mg
M	molecular mass, kg/kmol	Z	critical compressibility factor, dimensionless
m_i	melting enthalpy group contribution parameter, dimensionless	α_{th}	thermal diffusivity, m^2/s
M_j	occurrence of group j in a molecule, dimensionless	ΔH_f	latent heat of fusion, J/kg
N	number of molecules in a system, dimensionless	ΔH_m	total enthalpy of melting, J/mol
N_{atoms}	number of atoms, dimensionless	ΔS_m	total entropy of melting, $\text{J}/(\text{mol K})$
N_A	Avogadro's number, kmol^{-1}	ε	molecular eccentricity, dimensionless
n_i	occurrence of group i in a molecule, dimensionless	$\theta_{rot,m}$	rotational temperature, K
N_k	occurrence of group k in a molecule, dimensionless	λ	thermal conductivity, $\text{W}/(\text{m K})$
pck	critical pressure group contribution parameter, dimensionless	λ_f^*	reduced thermal conductivity correction term, dimensionless
		λ_m^*	reduced thermal conductivity of a monatomic liquid, dimensionless
		ζ	number of molecular degrees of freedom, dimensionless
		ρ	mass density, kg/m^3
		σ	molecular symmetry, dimensionless
		τ	molecular flexibility, dimensionless
		ω	acentric factor, dimensionless

liquid phase properties of organic PCMs on the right-hand side of Eq. (1) are readily available [20,21], but gaps exist in available data. Furthermore, the gaps in liquid-phase properties cannot be filled by equivalent solid phase properties since the shifted molecular arrangement between solid and liquid phases could have a dramatic influence on the thermophysical properties in the following ways through a loss of a molecular lattice structure:

- The lattice configuration contains a strong influence on the scattering mechanisms in phonon behavior in thermal conduction.
- Losing the lattice structure adjusts the available effective degrees of freedom of the molecules, thereby altering the specific heat.
- A loss in lattice structure affects the molecular packing arrangement, influencing the material density.

Furthermore, a PCM ideally exists in its liquid phase during one half of a heating/cooling cycle, and therefore an accurate model of the thermal response of the PCM should apply the liquid phase thermal properties, especially during a freezing process. However, many investigators have either ignored thermal gradients within the PCM [9] or assumed that the solid and liquid properties are

equivalent in numerical investigations [10,12,22]. Therefore, this study aims at determining accurate predictive techniques of liquid phase thermophysical properties for two principal classes of organic PCMs: alkanes and unsaturated (fatty) acids.

This study is intended to supplement the large body of work on PCM enhancement using nanoscale inclusions. Several studies [23–27] investigated the impact of adding highly-conducting nanoscale inclusions into a base organic PCM. In general, researchers have found that these composites contain significant conductivity enhancement (in general >100% enhancement for >1 wt% filler) but with a sacrifice in the latent enthalpy of fusion (~7–15% reduction for typical loading values). Fan et al. [26] compared different fillers and found that graphene nanoplatelets and short cylindrical inclusions (e.g., carbon nanotubes) provide better conductivity enhancement than long inclusions. The limiting factor in PCM nano-composite performance is the combination of thermal properties associated with the base PCM, and therefore improving the thermal properties of the base PCM – the focus of this effort – will lead to more effective PCM nano-composites.

A number of theoretical techniques exist to determine various properties of liquids including critical temperature (T_c), critical

pressure (P_c), melting point (T_m), normal boiling point (T_b), acentric factor (ω), the latent heat of fusion (ΔH_f), and the properties listed in Eq. (1). These techniques include a variety of predictive methods [28] and those stemming from statistical thermodynamics (e.g., [29–32]). Therefore, this study examines various combinations of theoretical techniques that lead to thermal diffusivity predictions.

The path to predicting thermal diffusivity begins with the use of group/bond contribution theories to provide estimates of the boiling point temperature, critical point properties, the melting point temperature and latent heat of melting. Joback and Reid [33] developed a holistic approach to predicting a variety of thermophysical properties including boiling point, melting point, and critical properties by including the effects of hydrocarbon atomic groups containing oxygen, fluorine, and nitrogen atoms. Their approach was later updated by Constantinou and Gani [34], who combined the first-order approach of Joback–Reid with second-order molecular groups for improved accuracy. In addition, several investigators provide means to predict properties for a specific organic molecular group. For example, Teja et al. [35] developed empirical formulae for critical properties of alkanes and alkanols based on their experiments on these compounds with less than 19 carbon atoms. Furthermore, Magoulas and Tassios [36] combine empirical formulae with statistical thermodynamics to extrapolate values of critical properties, boiling points, vapor pressures, liquid densities, and enthalpies of vaporization to alkanes with more than 20 carbon atoms. Tsonopoulos [37] provides a thorough listing of experimentally-determined critical constants for various alkanes (≤ 20 carbon atoms) along with known correlations. He created correlations for these data and extrapolated to determine the critical properties at infinite alkane chain lengths. Marrero–Morejón and Pardillo–Fontdevila [38] enhanced an earlier bond-based group theory [39] as an alternative to the atomic group-based theories by Joback–Reid and Constantinou–Gani. Finally, work by Yalkowsky et al. [40–43] uses group theory and molecular information to determine melting and boiling temperatures. This study considers group theory methods by Joback and Reid [33], Constantinou and Gani [34], and Marrero–Morejón and Pardillo–Fontdevila [38] for prediction of critical properties and boiling point temperature. In addition, the Joback–Reid and Constantinou–Gani methods provide melting point temperature, with the former also providing the enthalpy of fusion. Finally, the Yalkowsky approach is used for predictions of both melting and boiling temperatures.

A number of methods also exist for thermal conductivity prediction, heat capacity, and enthalpy of fusion. The text by Poling et al. [28] provides a number of simple empirical methods for thermal conductivity prediction, and those by Latini et al. [44,45], Poling et al. [28], Arikol and Gurbuz [46], and Sato–Riedel [28,47] are used in this study. The heat capacity was predicted using the group contribution methods of Růžička et al. [48] and Chueh and Swanson [49], along with the statistical thermodynamic approach discussed below. The enthalpy of fusion, although not used in Eq. (1), is nevertheless an important parameter in PCM thermal analysis and is therefore examined using methods by Joback and Reid [33], Dannerfeller and Yalkowsky [50], and Lian and Yalkowsky [51].

The acentric factor, which is used to determine the liquid density when a statistical thermodynamic fluid model is implemented, was found using statistical thermodynamics as discussed below. The correlation in the text by Poling et al. [28] was also used for comparison. The latter method is based on the three parameter Pitzer et al. [52] expansion with analytical expressions developed by Ambrose and Walton [53], and it requires inputs of critical temperature and pressure, as well as the normal boiling point.

The saturated liquid density can be found using a number of different methods. Gunn and Yamada [54] created a method based on the simple method by Rackett [55] that calculates the density

based on a simple expression containing the reduced pressure and critical point compressibility. The text by Poling et al. [28] provides an additional variation on the Rackett method. In addition, Elbro et al. [56] uses a group contribution method for liquid density prediction. The method by Hankinson and Thomson [57] uses the reduced temperature, critical temperature and pressure, and acentric factor. These methods are used along with the statistical thermodynamic approach below.

A number of these predictive techniques rely on other property inputs, and therefore the errors in predictive techniques can build upon each other, leading to grossly erroneous results. Therefore, this study examines an approach that determines the best path to prediction (BPP), or the combination of available predictive techniques that provides the best agreement with experimental data, for both alkanes and unsaturated acids. Experimental measurements are also employed to supplement existing property data to enable the calibration of the BPP. Knowledge of the BPP for a group of similar molecules (e.g., alkanes) enables researchers to explore the influence of tweaking the PCM molecular structure on predicted bulk thermophysical properties, thereby allowing for the creation of better-performing PCMs.

The approach proposed here is unique to the common practice of enhancing existing models to improve the accuracy of thermophysical property predictions. While a need exists to apply effort in the development and refining of new thermophysical property predictive models, this is not the focus of the work here. Instead, the goal here is to develop an optimal predictive pathway to property determination, which is still practical even though it does not use the former approach. It should be pointed out that all methods discussed in this article contain a physical basis but also employ approximations that lead to inaccuracies, and the goal of the statistical method used here is to limit those inaccuracies mathematically.

A substantial number of methods exist for the prediction of properties in Eq. (1), and therefore only a representative subset is used in this study. The choice of methods used here is based primarily on ease of use, accessibility of data, and diversity, with the hypothesis that the statistical mean of the various predictions for each property is similar to its experimentally-determined respective value. Therefore, it is anticipated that the exact selection of which methods to use is not as important as the implementation of a variety of approaches.

Finally, it must be mentioned that the predictions applied here are focused at the melting temperature as the standard of range of PCM operation is generally within a few degrees of this temperature. The errors associated with the BPP technique and experimental measurements will generally be larger than that associated with the temperature dependence of thermal properties. Therefore, the use of a BPP technique is intended solely for the modeling of PCM behavior for engineering design purposes.

2. Statistical thermodynamic approach

In this study, statistical thermodynamics uses inputs of critical properties and boiling and melting point temperatures to compute the acentric factor, heat capacity, and liquid density. The approach to predicting the three output properties requires the use of thermodynamic property calculations stemming from the canonical partition function, Q , which is known for a variety of cubic equations of state:

- Van der Waals [31]

$$Q = \frac{\pi^{(\frac{\epsilon-5)N}{2}}}{\sigma^N N!} \left(\frac{2\pi M k_B T (V - Nb_V)^{2/3}}{h^2} \right)^{3N/2} \left(\frac{T}{\theta_{rot,m}} \right)^{\frac{(\epsilon-3)N}{2}} \exp \left(\frac{a_V N^2}{V k_B T} \right) \quad (2)$$

- Redlich–Kwong [58]

$$Q = \frac{\pi^{(\xi-5)N}}{\sigma^N N!} \left(\frac{2\pi M k_B T (V - Nb_R)^{2/3}}{h^2} \right)^{3N/2} \left(\frac{T}{\theta_{rot,m}} \right)^{\frac{(\xi-3)N}{2}} \left(\frac{V + Nb_R}{V} \right)^{\left(\frac{a_R N}{b_R k_B T^{3/2}} \right)} \quad (3)$$

- Soave–Redlich–Kwong [59]

$$Q = \frac{\pi^{(\xi-5)N}}{\sigma^N N!} \left(\frac{2\pi M k_B T (V - Nb_S)^{2/3}}{h^2} \right)^{3N/2} \left(\frac{T}{\theta_{rot,m}} \right)^{\frac{(\xi-3)N}{2}} \left(\frac{V + Nb_S}{V} \right)^{\left(\frac{a_S \alpha_S N}{b_S k_B T} \right)} \quad (4)$$

- Peng–Robinson [60]

$$Q = \frac{\pi^{(\xi-5)N}}{\sigma^N N!} \left(\frac{2\pi M k_B T (V - Nb_P)^{2/3}}{h^2} \right)^{3N/2} \left(\frac{T}{\theta_{rot,m}} \right)^{\frac{(\xi-3)N}{2}} \left(\frac{V + (1 + \sqrt{2})Nb_P}{V + (1 - \sqrt{2})Nb_P} \right)^{\left(\frac{a_P \alpha_P N}{2\sqrt{2}b_P k_B T} \right)} \quad (5)$$

In the above equations, ξ is the number of degrees of freedom in the molecule, σ is the symmetry factor, N is the number of molecules in the system, M is the molecular mass, k_B is Boltzmann's constant, T is temperature, h is Planck's constant, V is volume, and $\theta_{rot,m}$ is the rotational temperature. The coefficients a , b , and α are fluid model-dependent, while the subscripts V , R , S , and P refer to the van der Waals, Redlich–Kwong, Soave–Redlich–Kwong, and Peng–Robinson fluid models, respectively.

In the above fluid models, only the parameter α depends on the acentric factor ω . Therefore, the van der Waals and Redlich–Kwong models are independent of ω and calculate only the liquid density and heat capacity. This is accomplished by determining the equilibrium reduced pressure ($P_r = P/P_c$) and reduced liquid and vapor densities at the reduced boiling point,

$$T_{rb} = \frac{T_b}{T_c} \quad (6)$$

where expressions for the chemical potential at T_{rb} and P_r are identical whether liquid or vapor densities are used [29,30].

The Soave–Redlich–Kwong and Peng–Robinson fluid models were analyzed differently due to their dependence on α . This additional parameter enables a matching of both T_{rb} and the reduced boiling point pressure

$$P_{rb} = \frac{P_0}{P_c} \quad (7)$$

where P_0 is 1 atm. The approach used here is to adjust the parameter α until liquid–vapor phase equilibrium was reached at T_{rb} and P_{rb} . These calibrated values of α are then related to the parameter f as

$$f = \frac{\sqrt{\alpha} - 1}{1 - \sqrt{T_{rb}}} \quad (8)$$

This acentric factor is then calculated by finding the roots of the fluid model-dependent function f :

$$f_S = 0.480 + 1.574\omega - 0.176\omega^2 \quad (9)$$

$$f_P = 0.37464 + 1.54226\omega - 0.26992\omega^2 \quad (10)$$

The molar heat capacity (\hat{c}_p) is calculated from the fluid models using

$$\begin{aligned} \hat{c}_p &= \left[\left(\frac{\partial H}{\partial T} \right)_{P,N} \right]_{N=N_A} \\ &= \left[\left(\frac{\partial H}{\partial T} \right)_{V,N} - \left(\frac{\partial H}{\partial V} \right)_{T,N} \left(\frac{\partial P}{\partial T} \right)_{V,N} \left(\frac{\partial P}{\partial V} \right)_{T,N}^{-1} \right]_{N=N_A} \end{aligned} \quad (11)$$

where H is the system enthalpy, P is pressure, and N_A is Avogadro's number. The enthalpy and pressure values are calculated from the canonical partition function Q using

$$P = k_B T \left(\frac{\partial (\ln Q)}{\partial V} \right)_{T,N} \quad (12)$$

$$H = U + PV = \frac{k_B T^2}{Q} \left(\frac{\partial Q}{\partial T} \right)_{V,N} + k_B T V \left(\frac{\partial (\ln Q)}{\partial V} \right)_{T,N} \quad (13)$$

where U is the system internal energy.

3. Predictive method combinations

For this work, the five common organic PCMs analyzed were heneicosane, tricosane, tetracosane, oleic acid, and linoleic acid. The first three PCMs are long, simple alkane chains, whereas the latter two are monounsaturated and polyunsaturated cis-isomer unsaturated acids. Fig. 1 shows the procedure used in this study, which consists of using 22 methods to solve for nine thermophysical properties of PCMs. These methods were arranged in a tiered hierarchy such that all thermophysical properties originate from only the molecular structure:

- **Tier 1:** The molecular structure was used as the initial input.
- **Tier 2:** Joback–Reid [33], Constantinou–Gani [34], and Marrero–Pardillo [38] methods were used to determine the critical temperature and pressure of the liquid based solely on molecular structure.
- **Tier 3:** The melting and boiling temperatures were predicted using the group contribution methods of Joback–Reid [33] and Constantinou–Gani [34] and the combined group contribution–molecular structure approach of Yalkowsky et al. [40–43]. The method of Marrero–Pardillo [38] was also used to solve for only the boiling temperature.
- **Tier 4:** The critical properties, melting temperature, and boiling temperature constituted the input parameters used to solve for the thermal conductivity, enthalpy of fusion, heat capacity, and acentric factor. Thermal conductivity was determined using methods by Latini et al. [44], Sastri et al. [28], and Riedel–Sato [28,47] based on the critical temperature, boiling point, and melting point. The method of Arikol and Gurbuz [46] applies these input parameters along with critical pressure. In addition, the Arikol method distinguishes between aliphatic and aromatic hydrocarbons, as well as monatomic molecules. Oleic acid and linoleic acid were assumed as aliphatic hydrocarbons, since they are carboxylic acids connected to aliphatic alkane chains. The enthalpy of fusion was predicted using the Joback–Reid method [33], the Dannenfelser–Yalkowsky [50] method, and the Lian–Yalkowsky method [51] using the enthalpy equation from [40,41]. The Joback–Reid method uses only the molecular structure, and the Dannenfelser–Yalkowsky the molecular structure and melting temperature. The method of Lian and Yalkowsky uses similar inputs as the Dannenfelser–Yalkowsky approach but with the addition of molecular eccentricity. Heat capacity was predicted using the Chueh–Swanson [49] and Růžička et al. [48] group contribution methods, and statistical thermodynamics. It should be noted that the Chueh–Swanson approach predicts the heat capacity at 293 K, which is not a significant deviation from the typical melting point of PCMs considered in this study.
- **Tier 5:** Density was predicted using the methods by Rackett [55], Gunn and Yamada [54], and the variation on the Rackett method as described by Poling et al. [28]. For clarity, the latter method is termed the “Modified Rackett” method in this study. Methods by Hankinson, Brobst, and Thomson [57], and Elbro

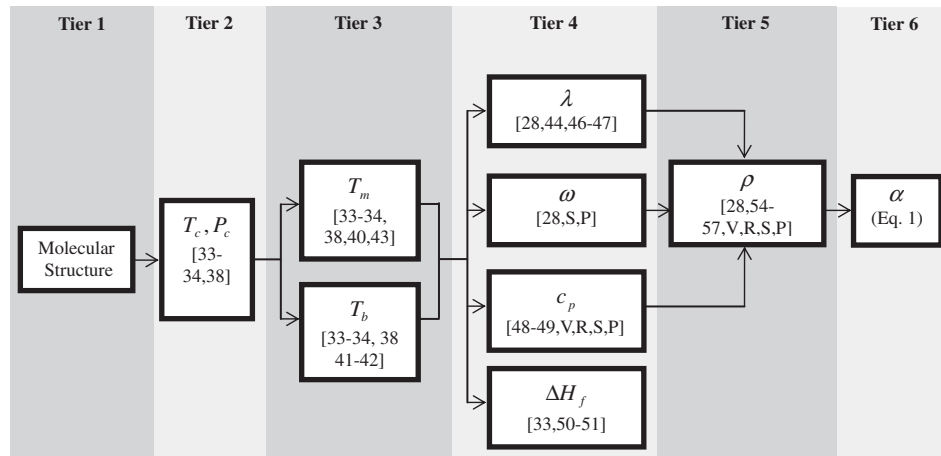


Fig. 1. Flowchart explaining the tier system of analysis used to predict PCM thermal properties. The methods used to predict each property are cited, and the letters V, R, S, and P refer to the use of the van der Waals, Redlich–Kwong, Soave–Redlich–Kwong, and Peng–Robinson fluid models, respectively.

et al. [56] are also used. Finally, the statistical thermodynamic approach was employed using each of the aforementioned four fluid models.

- **Tier 6:** Thermal diffusivity was calculated using Eq. (1). The BPP was defined as the most accurate α_{th} stemming from all possible combinations of λ , c_p and ρ from available pathways. For this project, the definition of accuracy in α_{th} was made on a group basis as described in the Results Section.

4. Experimental measurements

Experimental measurements on each PCM were performed to determine the thermophysical properties in the liquid phase to supplement values available in literature. Four PCMs (heneicosane, tricosane, tetracosane, and linoleic acid) were purchased at Fluka analytical grade per Sigma Aldrich, whereas oleic acid was technical grade. First, the melt temperatures of heneicosane, tricosane and tetracosane were found using differential scanning calorimetry (DSC). To obtain the melt temperature by DSC, a DSC Q200 instrument was programmed to apply a transient thermal ramp rate of 2 °C/min and the heat flow into the sample was recorded as a function of temperature. The heat flow response was measured using DSC at several different ramp rates and found that 2 °C/min gives us optimal resolution with respect to identifying and separating the solid–solid and solid–liquid phase transitions. Solid–liquid phase transitions are represented by endothermic peaks in the resultant curves. The melting temperature was defined to be the minimum of the primary endothermic peak.

The heat capacities of all five samples were also obtained using the DSC curves according to Ref. [61]. To do this, a DSC curve of a sapphire sample with well-defined temperature-dependent heat capacity was produced in order to obtain a reference calorimetric sensitivity $E(T)$, determined from ASTM E1269 as

$$E(T) = \left[\frac{g}{60D_{st}(T)} \right] [W_{st}c_{p,st}(T)] \quad (14)$$

where g represents the ramp rate, $D_{st}(T)$ is the difference in heat flow between an empty reference pan and the sapphire sample, W_{st} is the weight of the sapphire sample, and $c_{p,st}(T)$ is the heat capacity of the sapphire sample. The heat capacity of each PCM was calculated using $E(T)$ by

$$c_p(T) = \frac{60E(T)D_s(T)}{W_s g} \quad (15)$$

where D_s is the difference in heat flow between an empty reference pan and the sample of interest, and W_s is the weight of the sample

of interest. The latent heat of fusion was also found for each of the PCMs as the area above the primary endothermic peak, taking into account the solid–solid phase transition prior to melting. A linear fit was used that spanned from the maximum of the peak prior to the solid–liquid phase transition to the maximum of the peak after the solid–liquid phase transition. The range of values measured (200–300 kJ/kg) is consistent with other values in literature [62]. Fig. 2 provides the DSC curves used in this analysis for the three alkane organic PCMs.

The density of the unsaturated acids in their liquid phase was calculated by a simple weight/volume experiment. Each PCM was held at a temperature of 10 K above its melt temperature during the measurement using a flexible heater, and its weight was measured using a Denver Instruments balance accurate to ± 0.0001 mg. This temperature of the PCM was maintained above its melt temperature in order to ensure that the PCM was fully in its liquid phase, rather than in an intermediate, amorphous solid-phase. The volume was recorded using a graduated cylinder.

Each PCM's thermal conductivity was obtained using the transient plane source (TPS) technique. For these tests, a HotDiskAB TPS500 Thermal Constants Analyzer was vertically immersed in each PCM, which was held at 10 K above each corresponding melt temperature using a copper containment vessel and thermal bath, as described in the authors' previous work [63,64]. The TPS thermal characterization technique simultaneously solves for thermal conductivity and thermal diffusivity of materials using a sensor that acts as both a heat source and a temperature thermometer based

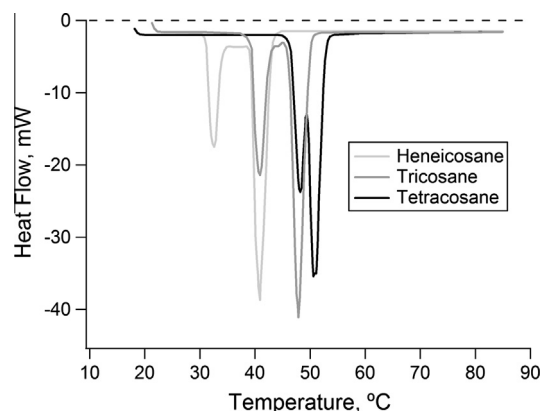


Fig. 2. DSC heating curves for heneicosane, tricosane, and tetracosane at a 10 °C/min ramp rate.

on basic resistance temperature detector (RTD) principles. The sensor is an infinitely thin, vertical cylinder constructed using a double-spiral nickel foil wire. In a typical measurement, the sensor is powered on and its average spatial temperature is recorded as a function of time. For a surrounding material with low thermal diffusivity, the average temperature rise across the sensor with respect to time is higher than one with a larger diffusivity. In order to calculate the thermal conductivity of the surrounding material, the transient temperature rise is inserted into a known mathematical expressions for transient heat conduction [65], where a semi-infinite boundary condition is imposed so the thermal penetration depth into the sample does not exceed the distance from the sensor to the material's edges.

Care was taken to ensure that natural convection across the sensor face was negligible during testing. The methodology described in the authors' previous work regarding the thermal characterization of liquids with the TPS technique is used in this study in order to ensure that natural convection across the sensor face does not occur during testing [63,64]. Additionally, the volumetric heat capacity obtained by the DSC experimentation and the density were used in the calculation of the thermal conductivity of the surrounding liquid-phase PCM in order to ensure a $\pm 5\%$ solution accuracy. The measurement time used to calculate the thermal conductivity and the probing depth of the thermal gradient were considered in order to ensure that the constraints set forth in Refs. [63,64] are met. The thermal diffusivity of each material is calculated according to Eq. (1). The uncertainty in thermal conductivity and thermal diffusivity are discussed in Ref. [64], and the uncertainty in DSC measurements is $\pm 2\%$ per the manufacturer. However, it must be noted that recent work suggests that long-term exposure by paraffins to temperatures above the melting point can cause a change in melting point and enthalpy of fusion, thereby potentially increasing the uncertainty based on environment [66].

5. Experimental results

Table 1 provides the experimentally-measured values of melting point temperature and latent heat of fusion for the alkanes using DSC. For calibration purposes the melting points for the alkanes are taken as their melting onset temperatures. The table also provides heat capacity measurements for all five materials using DSC. In addition, the table shows the measured thermal conductivity values of all PCMs using TPS, the reported values of density for the alkanes, and measured values of density using the weight/volume experiment for the unsaturated acids. The use of DSC to determine T_m and c_p for the unsaturated acids was not viable since they are liquid at room temperature and the equipment used did not have the capability to run tests at subambient temperatures. The table shows that the melting point increases with increasing numbers of atoms for the alkane chains, which is consistent with numerous other hydrocarbons [61]. The data shows that

the unsaturated acids contain a substantially lower heat capacity than the alkane chains, which is likely due to the fewer available degrees of freedom within the molecule due to the presence of fewer atoms. Surprisingly, tricosane showed a smaller heat capacity and thermal conductivity but a larger heat of fusion than the other alkane chains, and the reason for this requires further exploration. The table states that the density values of unsaturated acids tend to be much larger than the alkane chains, which is expected since the unsaturated acids contain increased hydrogen bonding due to the presence of OH groups. Finally, the thermal conductivity of alkane chains appears to be larger than the unsaturated acids, with the potential explanation that the uniform single bonding seen in alkane chains leads to less phonon scattering than in the double bonds seen in unsaturated acids.

6. Predictive results

Table 2 shows the statistical mean, median, and variance for all calculated properties using the aforementioned methods. The error in the table is defined based on deviation from the measured or reported value, and the percentage variance is based on the mean property value. The total number of paths to predicting thermal diffusivity for all materials was 349,920, which is decreased to 303,192 when predictions containing imaginary numbers are ignored. The table shows large variance values in data for all properties except thermal conductivity, but small errors in the statistical mean and median for critical point properties, melting and boiling temperatures of alkanes, and thermal conductivity of alkanes. This result suggests that the use of statistics with multiple methods provides reasonable estimates for the Tier 2 and 3 properties of alkanes shown in Fig. 1. Larger errors are seen for the enthalpy of fusion, heat capacity, and density for all materials, and the phase transition temperatures for unsaturated acids, which suggests that the use of additional tiers results in a decrease in reliability of applying statistical distributions when stacking multiple methods to obtain predictions. In most cases, similar errors are seen for the statistical mean and median of properties when compared to experimentally-measured or accepted values. However, some discrepancies between mean and median values exist, notably the heat capacity and density of unsaturated acids, which indicates that the presence of outlying predictions at large values. One can conclude from the table that the predicted values of most PCM thermophysical properties are highly sensitive to the chosen predictive techniques.

One issue that has arisen in property prediction of unsaturated acids is that the predictive methods do not account for isomerization of unsaturated acids, which could have a major impact on thermal properties. For example, the cis isomerization causes the compound to not pack as tightly because the structural configuration of cis isomers is kinked rather than straight, greatly influencing density. Elaidic acid, for example, is a trans isomer of oleic acid and has a melting temperature of 42–44 °C, which is greater than

Table 1
Reported and experimentally-measured thermophysical properties of various PCMs.

PCM	T_m (K) ^a	ΔH_f (kJ/kg) ^a	c_p (J/kg K) ^a	ρ (kg/m ³) ^b	λ (W/m K) ^b
Heneicosane	312.3–316.7	294.6	2386	772.0 ^d	0.145
Tricosane	319.3–323.8	302.5	2181	777.6 ^d	0.124
Tetracosane	322.5–326.8	207.7	2924	773.6 ^d	0.137
Oleic acid	N/A ^c	N/A ^c	1744	870.60 \pm 4.33	0.103
Linoleic acid	N/A ^c	N/A ^c	1917	902.49 \pm 4.98	0.087

^a The measurement error in measured melt temperature, latent heat of fusion, and heat capacity is $\pm 10\%$.

^b The measurement error in measured thermal conductivity is $\pm 5\%$.

^c Not measured since the melt temperature is less than ambient, and the DSC equipment used does not have a subambient adapter.

^d Ref. [68].

^e Measured just above the PCM's melting temperature.

Table 2
Statistical analysis of organic PCM thermophysical properties and comparison to measured values.

PCM	Quantity	T_c (K)	Error (%)	P_c (MPa)	Error (%)	T_m (K)	Error (%)	T_b (K)	Error (%)
Heneicosane	Mean	805	3.47	974	5.44	314	0.641	634	0.635
	Median	798	2.57	973	5.53	315	0.962	625	0.794
	Variance	880		291×10^3		129		661	
Tricosane	Measured					312			
	Reported	778 ^a		1030 ^a				630 ^e	
	Mean	842	6.58	871	4.81	326	2.19	659	0.919
	Median	833	5.44	867	5.25	322	0.940	651	0.306
Tetracosane	Variance	1900		410×10^3		283		1070	
	Measured					319			
	Reported	790 ^a		915 ^a				653 ^e	
	Mean	860	7.50	826	4.62	333	3.10	673	1.20
Oleic acid	Median	852	6.50	821	5.20	324	0.310	663	0.301
	Variance	2580		469×10^3		404		1390	
	Measured					323			
	Reported	800 ^a		866 ^a				665 ^e	
Linoleic acid	Mean	876	N/A	1300	6.12	368	28.2	655	32.3
	Median	857	N/A	1270	3.67	336	17.1	627	26.7
	Variance	3600		223×10^4		3240		2480	
	Measured								
PCM	Reported	N/A ^b		N/A ^b		287 ^c		495 ^c	
	Mean	882	N/A	1340	9.39	357	34.7	633	53.6
	Median	863	N/A	1320	7.76	335	26.4	627	52.2
	Variance	3940		258×10^4		4020		5690	
PCM	Reported	N/A ^b		N/A ^b		265 ^d		412 ^f	
	Quantity	λ (W/m K)	Error (%)	ΔH_f (kJ/kg)	Error (%)	c_p (kJ/kg K)	Error (%)	ρ (kg/m ³)	Error (%)
	Mean	0.132	8.97	207	29.8	2.09	12.6	541	29.9
	Median	0.138	4.83	220	25.4	2.13	10.9	474	38.6
Heneicosane	Variance	0.999×10^{-3}		8.23×10^5		22.7		1.28×10^5	
	Measured	0.145		295		2.39			
	Reported							772 ⁱ	
	Mean	0.127	2.42	213	29.7	2.09	4.13	483	37.9
Tricosane	Median	0.133	7.26	222	26.7	2.13	2.29	432	44.5
	Variance	1.37×10^{-3}		1.07×10^6		26.9		1.76×10^5	
	Measured	0.124		303		2.18			
	Reported							778 ⁱ	
Tetracosane	Mean	0.126	8.03	216	3.85	2.09	28.4	503	35.0
	Median	0.130	5.11	223	7.21	2.11	27.7	413	46.6
	Variance	1.66×10^{-3}		1.21×10^6		30.7		1.93×10^5	
	Measured	0.137		208		2.92			
Oleic acid	Reported							774 ⁱ	
	Mean	0.139	35.0	207	47.9	2.37	36.2	845	2.96
	Median	0.132	28.2	187	33.6	1.93	10.9	542	37.8
	Variance	3.99×10^{-3}		1.07×10^6		1460		2.03×10^7	
Linoleic acid	Measured	0.103				1.74		871	
	Reported			140 ^g					
	Mean	0.136	56.3	198	16.5	2.34	21.9	851	5.65
	Median	0.128	47.1	189	11.2	1.90	1.04	522	42.1
PCM	Variance	5.10×10^{-3}		9.83×10^5		1520		1.93×10^7	
	Measured	0.087				1.92		902	
	Reported			170 ^h					

^a Ref. [69]. Uncertainty in T_c and P_c are ± 3 K and ± 0.04 MPa, respectively.

^b No reliable source available.

^c Ref. [70].

^d Ref. [71].

^e Ref. [72].

^f Ref. [73].

^g Ref. [74].

^h Ref. [75].

ⁱ Ref. [68].

the melting temperature of cis oleic acid of 13–14 °C [61]. Recent work by Wang et al. [67] has added new structure factors to their predictive equations to account for trans and cis isomerization. Wang's method could not be used in this study, however, as it cannot account for all of the position group contributions of linoleic acid, which includes a carbon bonded to two double bonded carbon atoms and two hydrogen atoms [C-(Cd)₂(H)₂]. However, Wang's method provides a promising avenue for improved predictions of thermophysical properties that account for isomerization.

Histograms of thermal diffusivity predictions are shown in Figs. 3–7 for the five materials. All materials show a normal

distribution of predictions, with all except heneicosane including some negative values. The results show that increasing the number of atoms results in more outliers in the distribution in both directions, and the unsaturated acids contain more outliers than the alkane chains. The experimentally-measured value appears to the left of the peak in the normal distribution, showing that most pathways to prediction over-predict the thermal diffusivity. Therefore, one cannot use the statistics ascertained from a large set of combining different predictive methods to achieve reasonable approximations of thermal diffusivity, and therefore a BPP must be considered instead.

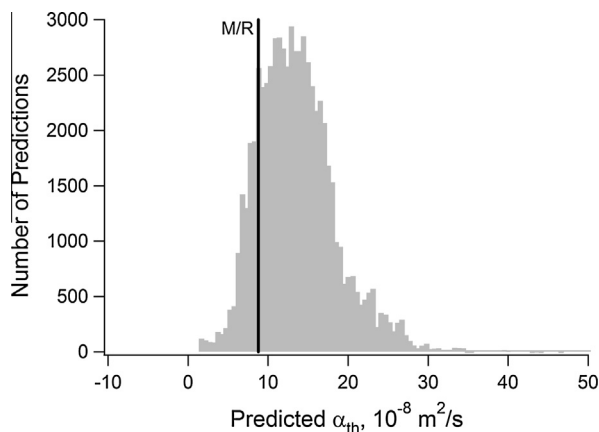


Fig. 3. Histogram of heneicosane thermal diffusivity predictions and experimentally-measured/reported value.

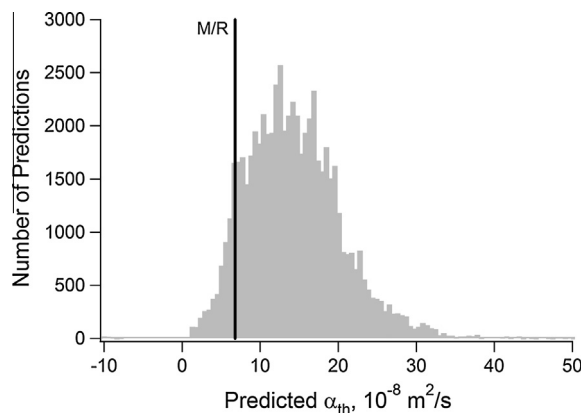


Fig. 6. Histogram of oleic acid thermal diffusivity predictions and experimentally-measured/reported value.

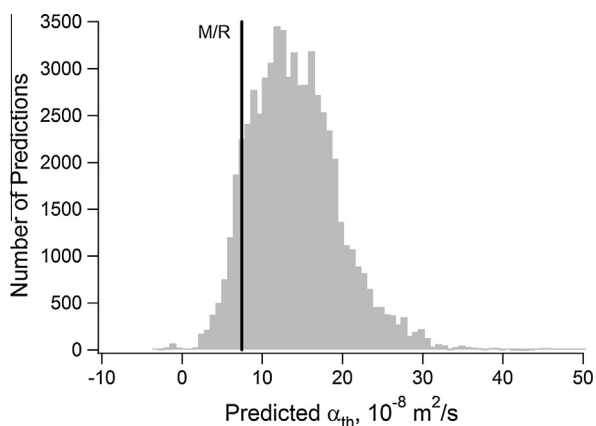


Fig. 4. Histogram of tricosane thermal diffusivity predictions and experimentally-measured/reported value.

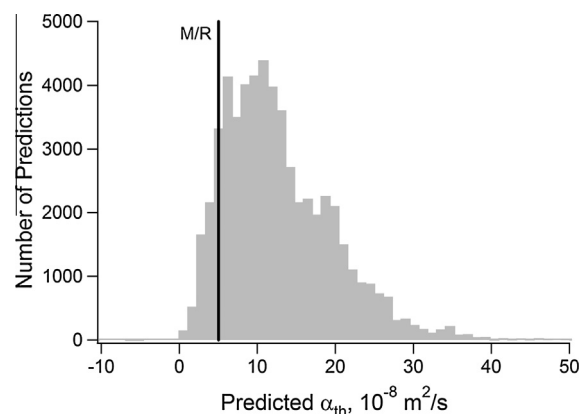


Fig. 7. Histogram of linoleic acid thermal diffusivity predictions and experimentally-measured/reported value.

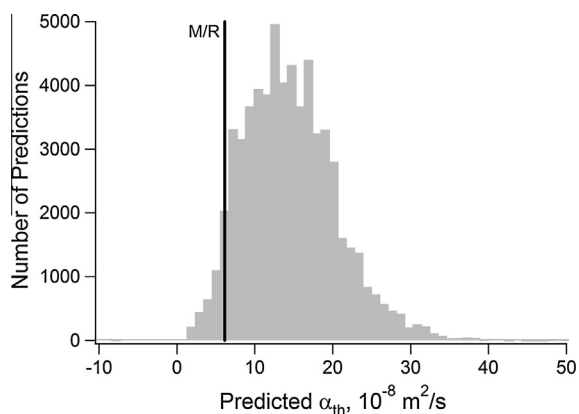


Fig. 5. Histogram of tetracosane thermal diffusivity predictions and experimentally-measured/reported value.

Unsaturated acids do not share a similar molecular makeup as the alkane chains because of isomerization. Therefore, a BPP for the entire group of all five materials was not created and instead BPPs for the two groups of organic PCMs (alkane chains and unsaturated acids) were explored instead. Table 3 provides the BPP sequence for thermal diffusivity prediction of alkane chain-based organic PCMs by minimizing the average error in thermal diffusivity prediction for heneicosane and tetracosane. The table also

shows the thermal property predictions for tricosane. The results show similar predictions in properties for all three materials, and that predictions of individual properties along the BPP sequence can have significant errors when compared to experimental measurements, and therefore the BPP may only be applied to predict thermal diffusivity and not intermediate values. The primary equations associated with group theory-based BPP calculations are provided in Table 4, and the acentric factor was calculated using the Soave–Redlich–Kwong fluid model.

Table 5 similarly provides a BPP for thermal diffusivity for unsaturated acids based on the minimal average error in thermal diffusivity for oleic acid and linoleic acid. Again, the BPP for thermal diffusivity does not necessarily contain the most accurate individual predictions of thermal conductivity, heat capacity, or density; for it is possible that the combination of the inaccuracies in individual properties may result in a more accurate prediction of α_{th} per Eq. (1). Table 4 provides the major equations associated with the group theory-based methods in the BPP, whereas the density was calculated using the Redlich–Kwong fluid model.

Table 6 provides predictions of thermal diffusivity using the statistical mean and median values of predictions from Table 2 along with the BPPs in Tables 3 and 5. The BPPs provide very good (<2%) accuracy for heneicosane and tetracosane since they are used in the calibration process. The application of the BPP on tricosane shows an error of approximately 9%, which therefore provides a representative uncertainty in the application of the BPP for alkane chains similar to heneicosane and tetracosane. The BPP for unsaturated acids provides good agreement for oleic acid yet only 10%

Table 3
BPP intermediate values for predicting paraffin alkane chain thermal diffusivity.^a

Property: Method:	T_c (K) [33]	P_c (MPa) [33]	T_m (K) [34]	T_b (K) [41]	λ (W/m K) [46]	c_p (kJ/kg K) [48]	ω () S^d	ρ (kg/m ³) [54]
Heneicosane ^b	842	956	299	625	0.0703	2.17	2.11×10^{-1}	416
Tetracosane ^b	918	806	313	663	0.0473	2.21	6.88×10^{-2}	348
Tricosane ^c	892	852	309	651	0.0542	2.20	-4.77×10^{-4}	369

^a Results using this path to prediction are shown in Table 5.

^b Material used to calibrate BPP.

^c Material used to test BPP.

^d Statistical thermodynamics with the Soave–Redlich–Kwong fluid model.

Table 4
Primary equations used in group-based BPP predictive methods.

Fluid group	Property	Equation	Ref.
Alkanes, acids	T_c , K	$= T_b [0.584 + 0.965 \sum_k N_k (tck) - \{\sum_k N_k (tck)\}^2]$	[33]
Alkanes, acids	P_c , bar	$[0.113 + 0.0032 N_{atoms} - \sum_k N_k (pck)]^2$	[33]
Alkanes, acids	T_m , K	$= 102.425 \ln [\sum_k N_k (tfp1k) + W \sum_j M_j (tfp2j)]$	[34]
Alkanes	T_b , K	$\frac{\sum n_i m_i}{43.51 - 9.07 \log_{10} \sigma + 7.93 \tau + 9.58 \log_{10} \epsilon}$	[41]
Acids	T_b , K	$[\sum n_i b_i] / [87 + 0.35 \tau + 15 HBP]$	[42]
Alkanes	λ , W/(m K)	$(\lambda_m^* + \lambda_f^*) P_c^{2/3} T_c^{-1/6} M^{-1/2}$	[46]
Acids	λ , W/(m K)	$\frac{A^* T_b^z (1 - T_r)}{M^{\beta} T_c^y T_r^{1/6}}$	[44]
Alkanes, acids	C_{pb} , J/(mol K)	$= R [\sum_i n_i a_i + \frac{T}{100} \sum_i n_i b_i + (\frac{T}{100})^2 \sum_i n_i d_i]$	[48]
Alkanes	V_s , cm ³ /mol	$\frac{RT_c Z_c}{P_c} (0.29056 - 0.08775 \omega)^{(1 - T/T_c)^{2.7}}$	[54]

Table 5
BPP intermediate values for predicting unsaturated acid thermal diffusivity.^a

Property: Method:	T_c (K) [33]	P_c (MPa) [33]	T_m (K) [34]	T_b (K) [42]	λ (W/m K) [44]	c_p (kJ/kg K) [48]	ρ (kg/m ³) R^b
Oleic acid	943	1270	336	613	0.134	4.19	481
Linoleic acid	951	1320	335	539	0.116	4.26	492

^a Predictions using this path to prediction are shown in Table 5.

^b Statistical thermodynamics with the Redlich–Kwong fluid model.

agreement for linoleic acid, which means that the uncertainty in BPP predictions could be large even for those materials used in the calibration process.

The table also shows that average error for the alkane chains using the mean values of individual properties is significantly lower than using median values, which is unexpected since the mean values of individual properties do not consistently show better agreement in Table 2. Applying the mean values in oleic acid results in overpredictions of thermal conductivity and heat capacity, resulting in a surprisingly accurate thermal diffusivity prediction. However, linoleic acid could not be predicted effectively with statistical variables.

The alkane and fatty acid BPPs were applied on similar materials to test their reliability. The alkanes and fatty acids were chosen based on available data and the practicality of their use as PCMs per their melting point values. Table 7 shows that the alkane-based BPP is reliable within ~15% for alkanes down to a chain length of 18–24 carbon atoms. In addition, the fatty acid-based BPP is also reliable within ~15% for fatty-acids with a chain length of 10–18 carbon atoms. Therefore the use of these BPPs is reasonable for thermal diffusivity prediction for a set of similar materials in their respective BPPs.

An accurate BPP for a group of organic PCMs can enable researchers to explore the influence of molecular structure on desired thermal properties. For example, Table 7 shows that the

Table 6
Comparison between theoretical predictions and experimental measurements/reported values of thermal diffusivity.

PCM	Quantity	α_{th} (m ² /s)	Error (%)
Heneicosane	Mean	1.17×10^{-7}	48.9
	Median	1.37×10^{-7}	74.3
	BPP ^a	7.81×10^{-8}	0.636
	M/R ^b	7.86×10^{-8}	
Tricosane	Mean	1.26×10^{-7}	72.4
	Median	1.45×10^{-7}	98.4
	BPP ^a	6.68×10^{-8}	8.62
	M/R ^b	7.31×10^{-8}	
Tetracosane	Mean	1.20×10^{-7}	98.0
	Median	1.49×10^{-7}	146
	BPP ^a	6.13×10^{-8}	1.16
	M/R ^b	6.06×10^{-8}	
Oleic acid	Mean	6.93×10^{-8}	2.22
	Median	1.26×10^{-7}	86.2
	BPP ^c	6.67×10^{-8}	1.67
	M/R ^b	6.78×10^{-8}	
Linoleic acid	Mean	6.86×10^{-8}	36.5
	Median	1.29×10^{-7}	156
	BPP ^c	5.53×10^{-8}	10.0
	M/R ^b	5.03×10^{-8}	

^a Best path to prediction from Table 3.

^b Experimentally-measured/reported values of λ , c_p , and ρ from Table 1.

^c Best path to prediction from Table 5.

Table 7
BPP predictions for various materials.

Property:	λ (W/m K)	c_p (kJ/kg K)	ρ (kg/m ³)	α_{th} (10 ⁻⁸ m ² /s)	α_{th} (10 ⁻⁸ m ² /s)	Error (%)
Method:	[M/R] ^a	[M/R] ^a	[M/R] ^a	[M/R] ^a	[BPP]	
Octadecane	0.146 ^c	2.22 ^d	775 ^e	8.46	9.41	10.1
Nonadecane	0.146 ^c	2.22 ^d	772 ^e	8.52	8.90	4.46
Eicosane	0.147 ^c	2.21 ^d	776 ^e	8.57	8.37	2.33
Heneicosane	0.145 ^f	2.39 ^f	772 ^b	7.86	7.81	0.636
Docosane	0.148 ^c	2.23 ^d	775 ^b	8.56	7.24	15.4
Tricosane	0.124 ^f	2.18 ^f	778 ^b	7.31	6.68	8.62
Tetracosane	0.137 ^f	2.92 ^f	774 ^b	6.06	6.13	1.16
Capric acid	0.153 ^g	2.1 ^g	878 ^g	8.29	8.06	2.77
Lauric acid	0.147 ^g	2.3 ^g	862 ^g	7.41	7.79	5.13
Myristic acid	0.150 ^g	2.4 ^g	861 ^g	7.26	7.69	5.92
Palmitic acid	0.162 ^g	2.8 ^g	850 ^g	6.81	7.71	13.2
Stearic acid	0.172 ^g	2.2 ^g	848 ^g	9.22	7.80	15.4
Oleic acid	0.103 ^f	1.74 ^f	871 ^f	6.78	6.67	1.67
Linoleic acid	0.087 ^f	1.92 ^f	902 ^f	5.03	5.53	10.0

^a Measured/reported.

^b [76].

^c [77].

^d [78].

^e [79].

^f Experimentally-measured values from Table 1.

^g [80].

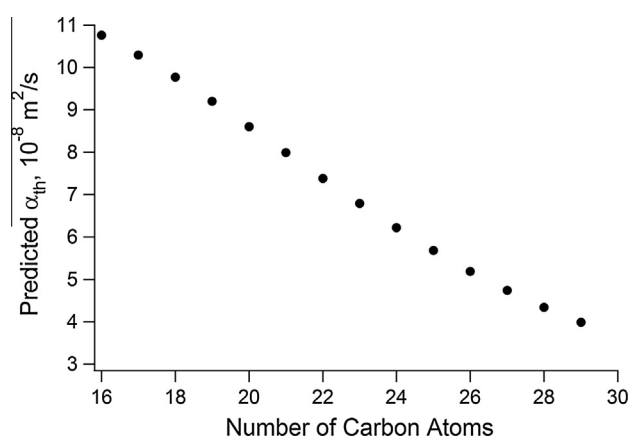


Fig. 8. Application of the optimal thermal diffusivity path to prediction for heneicosane, tricosane, and tetracosane to ascertain the influence of chain length on liquid thermal diffusivity.

alkane BPP is accurate within 15% for the shown range of alkane chains, so the BPP has been extrapolated to include shorter and longer chains to predict the influence of chain length on thermal diffusivity. This new predictive region spans from alkanes containing between 16 and 29 carbon atoms. Fig. 8 shows that the BPP suggests that doubling the length of the alkane chain reduces the alkane liquid phase thermal diffusivity by a factor of about 2.5.

7. Concluding remarks

Three important conclusions can be gained from this work. First, predictions of thermophysical properties of materials are strongly dependent upon the choice of method, and the variance in predictions grow exponentially with derived quantities (larger than Tier 2 in Fig. 1) such as thermal diffusivity. Second, the use of the statistical mean of a large set of predictive methods provides a reasonable prediction for alkane critical point properties, melting and boiling temperatures, and thermal conductivity. However, the use of statistics fails for unsaturated acids and all derived quantities. The lack of statistical accuracy requires the use of a BPP approach to provide accurate estimations of derived quantities for materials with similar molecular structures.

The BPPs provided in this study for paraffin alkane chains and unsaturated acids show that accurate predictions of liquid phase thermal diffusivity for phase change materials may be achieved, which is an important step in the goal of tailoring the molecular structure of materials to achieve optimal energy storage performance. For example, the described procedure towards determining a BPP may be tailored to different sets of phase change materials, which provides a starting point towards the development of new PCMs and other fluids. Although here the BPPs are focused solely on thermal diffusivity, future work will uncover unique BPPs for all relevant thermophysical properties for a given PCM application. This suite of BPPs will then be incorporated into device-scale simulations to predict the PCM energy storage capability based on molecular configuration. Thus, one may apply the methods described in this study to achieve multi-scale optimization of PCM systems, thereby improving the energy storage capability of portable electronics, building thermal envelopes, and sources of sustainable energy.

Acknowledgements

Preliminary work by Michael Meizoso is appreciated. This material is based upon work supported by the National Science Foundation under Grant No. CBET-1235769. Any opinions, findings, and conclusions or recommendations expressed in this material are those of the author(s) and do not necessarily reflect the views of the National Science Foundation.

References

- [1] Long J.-Y. Numerical and experimental investigation for heat transfer in triplex concentric tube with phase change material for thermal energy storage. *Sol Energy* 2008;82:977–85.
- [2] Veerappan M, Kalaiselvam S, Iniyan S, Goic R. Phase change characteristic study of spherical PCMs in solar energy storage. *Sol Energy* 2009;83:1245–52.
- [3] Hoshi A, Mills DR, Bittar A, Saitoh TS. Screening of high melting point phase change materials (PCM) in solar thermal concentrating technology based on CLFR. *Sol Energy* 2005;79:332–9.
- [4] Trp A. An experimental and numerical investigation of heat transfer during technical grade paraffin melting and solidification in a shell-and-tube latent thermal energy storage unit. *Polymeric materials for solar energy applications*. 6th ed. Elsevier Ltd; 2005. p. 648–60.
- [5] Medina MA, King JB, Zhang M. On the heat transfer rate reduction of structural insulated panels (SIPs) outfitted with phase change materials (PCMs). *Energy* 2008;33:667–78.

- [6] Kenisarin M, Mahkamov K. Solar energy storage using phase change materials. *Renew Sust Energy Rev* 2007;11:1913–65.
- [7] Wang Y, Tang B, Zhang S. Organic, cross-linking, and shape-stabilized solar thermal energy storage materials: a reversible phase transition driven by broadband visible light. *Appl Energy* 2014;113:59–66.
- [8] Neepfer DA. Thermal dynamics of wallboard with latent heat storage. *Sol Energy* 2000;68:393–403.
- [9] Guobing Z, Yinping Z, Qunli Z, Kunping L, Hongfa D. Performance of a hybrid heating system with thermal storage using shape-stabilized phase-change material plates. *Appl Energy* 2007;84:1068–77.
- [10] Athienitis AK, Liu C, Hawes D, Banu D, Feldman D. Investigation of the thermal performance of a passive solar test-room with wall latent heat storage. *Build Environ* 1997;32:405–10.
- [11] Na Z, Zhenjun M, Shengwei W. Dynamic characteristics and energy performance of buildings using phase change materials: a review. *Energy Convers Manage* 2009;50:3169–81.
- [12] Diaconu BM, Cruceru M. Novel concept of composite phase change material wall system for year-round thermal energy savings. *Energy Build* 2010;42:1759–72.
- [13] Cabeza LF, Castellón C, Nogués M, Medrano M, Leppers R, Zubillaga O. Use of microencapsulated PCM in concrete walls for energy savings. *Energy Build* 2007;39:113–9.
- [14] Castellón C, Medrano M, Roca J, Cabeza LF, Navarro ME, Fernández AI, et al. Effect of microencapsulated phase change material in sandwich panels. *Renew Energy* 2010;35:2370–4.
- [15] Eddahak-Ouni A, Drissi S, Colin J, Neji J, Care S. Experimental and multi-scale analysis of the thermal properties of Portland cement concretes embedded with microencapsulated Phase Change Materials (PCMs). *Appl Therm Eng* 2014;64:32–9.
- [16] Li M, Wu Z, Tan J. Heat storage properties of the cement mortar incorporated with composite phase change material. *Appl Energy* 2013;103:393–9.
- [17] Weinstein RD, Kopec TC, Fleischer AS, D'Addio E, Bessel CA. The experimental exploration of embedding phase change materials with graphite nanofibers for the thermal management of electronics. *J Heat Transfer* 2008;130:042405.
- [18] Vesligaj MJ, Amon CH. Transient thermal management of temperature fluctuations during time varying workloads on portable electronics. *IEEE Trans Compon Pack Technol* 1999;22:541–50.
- [19] Alawadhi EM, Amon CH. PCM thermal control unit for portable electronic devices: Experimental and numerical studies. *IEEE Trans Compon Pack Technol* 2003;26:116–25.
- [20] National Institute of Standards and Technology. NIST Chemistry WebBook. 2011.
- [21] Jankowski NR, McCluskey FP. A review of phase change materials for vehicle component thermal buffering. *Appl Energy* 2014;113:1525–61.
- [22] Duan X, Naterer GF. Thermal protection of a ground layer with phase change materials. *J Heat Transfer* 2010;132:011301 (9 pp.).
- [23] Warzoha RJ, Weigand RM, Fleischer AS. Temperature-dependent thermal properties of a paraffin phase change material embedded with herringbone style graphite nanofibers. *Appl Energy* 2014. <http://dx.doi.org/10.1016/j.apenergy.2014.03.091>.
- [24] Parameshwaran R, Deepak K, Saravanan R, Kalaiselvam S. Preparation, thermal and rheological properties of hybrid nanocomposite phase change material for thermal energy storage. *Appl Energy* 2014;115:320–30.
- [25] Zeng JL, Zheng SH, Yu SB, Zhu FR, Gan J, Zhu L, et al. Preparation and thermal properties of palmitic acid/polyaniline/exfoliated graphite nanoplatelets form-stable phase change materials. *Appl Energy* 2014;115:603–9.
- [26] Fan LW, Fang X, Wang X, Zeng Y, Xiao YQ, Yu ZT, et al. Effects of various carbon nanofillers on the thermal conductivity and energy storage properties of paraffin-based nanocomposite phase change materials. *Appl Energy* 2013;110:163–72.
- [27] Li M. A nano-graphite/paraffin phase change material with high thermal conductivity. *Appl Energy* 2013;106:25–30.
- [28] Poling BE, Prausnitz JM, O'Connell JP. The properties of gases and liquids. 5th ed. Boston (MA): McGraw-Hill; 2001.
- [29] Wemhoff AP. Extension of the neoclassical theory of capillarity to advanced cubic equations of state. *Int J Thermophys* 2010;31:253–75.
- [30] Carey VP. Thermodynamic properties and structure of the liquid-vapor interface: a neoclassical Redlich–Kwong model. *J Chem Phys* 2003;118:5053–64.
- [31] Rowlinson JS. Translation of J.D. van der Waals' "The thermodynamic theory of capillarity under the hypothesis of a continuous variation of density". *J Stat Phys* 1979;20:197–244.
- [32] Rowlinson JS, Widom B. Molecular theory of capillarity. Mineola (NY): Dover; 1982.
- [33] Joback KG, Reid RC. Estimation of pure-component properties from group-contributions. *Chem Eng Commun* 1987;57:233–43.
- [34] Constantinou L, Gani R. New group-contribution method for estimating properties of pure compounds. *AIChE J* 1994;40:1697–710.
- [35] Teja AS, Lee RJ, Rosenthal D, Anselme M. Correlation of the critical properties of alkanes and alkanols. *Fluid Phase Equilib* 1990;56:153–69.
- [36] Magoulas K, Tassios D. Thermophysical properties of n-alkanes from C1 to C20 and their prediction for higher ones. *Fluid Phase Equilib* 1990;56:119–40.
- [37] Tsoumpoulos C. Critical constants of normal alkanes from methane to polyethylene. *AIChE J* 1987;33:2080–3.
- [38] Marrero-Morejón J, Pardillo-Fontdevila E. Estimation of pure compound properties using group-interaction contributions. *AIChE J* 1999;45:615–21.
- [39] Pardillo-Fontdevila E, Gonzalez-Rubio R. A group-interaction contribution approach. A new strategy for the estimation of physico-chemical properties of branched isomers. *Chem Eng Commun* 1997;163:245.
- [40] Lian B, Yalkowsky SH. Molecular geometry and melting point related properties. *Ind Eng Chem Res* 2012;51:16750–4.
- [41] Lian B, Yalkowsky SH. Molecular geometry and boiling related thermodynamic properties. *J Chem Thermodyn* 2012;54:250–3.
- [42] Sanghvi R, Yalkowsky SH. Estimation of the normal boiling point of organic compounds. *Ind Eng Chem Res* 2006;45:2856–61.
- [43] Jain A, Yang G, Yalkowsky SH. Estimation of melting points of organic compounds. *Ind Eng Chem Res* 2004;43:7618–21.
- [44] Latini G. *Thermal Conduct* 1977;15:245.
- [45] Latini G, Sotte M. Thermal conductivity of refrigerants in the liquid state: a comparison of estimation methods. *Int J Refrig* 2012;35:1377–83.
- [46] Arikol M, Gurbuz H. A new method for predicting thermal-conductivity of pure organic liquids and their mixtures. *Can J Chem Eng* 1992;70:1157–63.
- [47] Riedel L. *Chem Eng Technol* 1949;21:349.
- [48] Růžička J, V. Záborský M, Malíjevký A, Domalski ES. Correlation of heat capacities of liquids as a function of temperature. *Fluid Phase Equilib* 1992;75:137–48.
- [49] Chueh CF, Swanson AC. Estimation of liquid heat capacity. *Can J Chem Eng* 1973;51:596–600.
- [50] Dannenfelser RM, Yalkowsky SH. Estimation of entropy of melting from molecular structure: a non-group contribution method. *Ind Eng Chem Res* 1996;35:1483–6.
- [51] Lian B, Yalkowsky SH. A simplified approach to predict the heat of melting for organic compounds. *Chemometr Intell Lab Syst* 2011;108:150–3.
- [52] Pitzer KS, Lippmann DZ, Curl RF, Huggins CM, Petersen DE. The volumetric and thermodynamic properties of fluids. 2. Compressibility factor, vapor pressure and entropy of vaporization. *J Am Chem Soc* 1955;77:3433–40.
- [53] Ambrose D, Walton J. *Pure Appl Chem* 1989;61:1395.
- [54] Gunn RD, Yamada T. A corresponding states correlation of saturated liquid volumes. *AIChE J* 1971;17:1341–5.
- [55] Rackett HG. Equation of state for saturated liquids. *J Chem Eng Data* 1970;15:514–7.
- [56] Elbro HS, Fredenslund A, Rasmussen P. Group contribution method for the prediction of liquid densities as a function of temperature for solvents, oligomers, and polymers. *Ind Eng Chem Res* 1991;30:2576–82.
- [57] Hankinson RW, Thomson GH. A new correlation for saturated densities of liquids and their mixtures. *AIChE J* 1979;25:653–63.
- [58] Redlich O, Kwong JNS. On the thermodynamics of solutions. 5. An equation of state – fugacities of gaseous solutions. *Chem Rev* 1949;44:233–44.
- [59] Soave G. Equilibrium constants from a modified Redlich–Kwong equation of state. *Chem Eng Sci* 1972;27:1197–203.
- [60] Peng D-Y, Robinson DB. A new two-constant equation of state. *Ind Eng Chem Fund* 1976;15:59–64.
- [61] Sigma Aldrich. Sigma Aldrich Product Catalog. Sigma Aldrich Product Catalog; Sigma Aldrich; 2013.
- [62] Sharma SD, Kitano H, Sagara K. Phase change materials for low temperature solar thermal applications. *Res Rep Fac Eng Mie Univ* 2004;29:31–64.
- [63] Warzoha RJ, Fleischer AS. Determining the thermal conductivity of liquids using the transient hot disk method. Part II: Establishing an accurate and repeatable solution method. *Int J Heat Mass Trans* 2014;71:790–807.
- [64] Warzoha RJ, Fleischer AS. Determining the thermal conductivity of liquids using the transient hot disk method Part I: Establishing transient thermal-fluid constraints. *Int J Heat Mass Trans* 2014;71:779–89.
- [65] He Y. Rapid thermal conductivity measurement with a hot disk sensor. Part I. Theoretical considerations. *Thermochim Acta* 2005;436:122–9.
- [66] Behzadi S, Farid MM. Long term thermal stability of organic PCMs. *Appl Energy* 2014;122:11–6.
- [67] Wang Q, Ma P, Neng S. Position group contribution method for estimation of melting point of organic compounds. *Chin J Chem Eng* 2009;17:468–72.
- [68] Grodzka PG. Study of phase-change materials for a thermal control system. Huntsville, Ala: Lockheed Missiles & Space Company; 1970.
- [69] Nikitin ED, Pavlov PA, Bessonova NV. Critical constants of n-alkanes with from 17 to 24 carbon atoms. *J Chem Thermodyn* 1994;26:177–82.
- [70] CAMEO Chemicals. Database of Hazardous Materials. In: National Oceanic and Atmospheric Administration, editor. 2013.
- [71] National Institutes of Health. PubChem. PubChem2013.
- [72] Weast RC, Grastelli JG. CRC handbook of data on organic compounds. 2nd ed. Boca Raton (FL): CRC Press, Inc.; 1989.
- [73] LookChem. LookChem. In: LookChem.com, editor. 2013.
- [74] Domalski ES, Hearing ED. Heat capacities and entropies of organic compounds in the condensed phase. Volume III. *J Phys Chem Ref Data* 1996;25:1–525.
- [75] Jalal IM, Zografí G, Rakshit AK, Gunstone FD. Thermal analysis of fatty acids. *Chem Phys Lipids* 1982;31:395–404.
- [76] Rastorguev YL, Bogatov GF, Grigorev BA. Thermal conductivity of higher n-alkanes. *Chem Technol Fuels Oils* 1974;10:54–8.
- [77] Engineering Sciences Data Unit. Thermal conductivity of liquids: Aliphatic hydrocarbons. Part 1. Alkanes. ESDU: 05020.
- [78] Engineering Sciences Data Unit. Heat capacity and enthalpy of liquids: Alkanes. ESDU: 86007.
- [79] Reid RC. Tables on the thermophysical properties of liquids and gases. 2nd ed. New York: Halsted Press; 1975.
- [80] Sharma A, Won LD, Buddhi D, Park JU. Numerical heat transfer studies of the fatty acids for different heat exchanger materials on the performance of a latent heat storage system. *Renew Energy* 2005;30:2179–87.